

2

Turbulent drop breakup in the flow of diluted O/W emulsions

This chapter reviews the published literature regarding the theories and experimental studies carried out on drop breakup phenomenon of diluted O/W macro emulsions (or simply emulsions) in turbulent flow. It is divided into two sections. First, emulsions fundamental principles and properties are introduced. Then, fundamentals of turbulence theory, drop breakup phenomenon and hydrodynamics in the two turbulent flows considered in this dissertation: Flow in a Rotor – Stator Mixer and Flow through an Orifice are presented. The literature review concentrates on aspects relevant to the resources used in the work of this dissertation.

2.1 Basic principles of emulsions

2.1.1 Fundamentals

Emulsions are fluids present in practically every stage of the petroleum production and recovery processes and must be faced during drilling, producing, transporting and processing crude oils. An emulsion is a liquid–liquid dispersion of naturally immiscible fluids, which exhibit certain persistence against phase separation because of the presence of stabilizing components, usually surfactants, at the interface. In most practical cases, they are considered as Surfactant-Oil-Water (SOW) systems, with at least three components. Surfactants or emulsifiers, have two main functions: to decrease the interfacial tension between phases; thereby enabling easier formation of the emulsion, and as already stated, to stabilize the dispersed phase against coalescence once it is formed (Pal, 2011).

Emulsions are categorized according to different criteria. In the classic type of emulsion, the two immiscible liquids involved are water and oil. Either of these two liquids can be defined as the dispersed phase. The dispersed phase is

sometimes designated to as internal phase, and the continuous phase as the external phase. Depending on which one is the dispersed phase, emulsions present reasonably different physical and rheological properties. The following types of emulsions are readily distinguished in principle:

- Oil in Water (O/W) for oil droplets dispersed in water,
- Water in Oil (W/O) for water droplets dispersed in oil,
- Oil in Water in Oil (O/W/O) and
- Water in Oil in Water (W/O/W).

The O/W/O and W/O/W emulsions are known as multiple emulsions and they are present in cases in which the dispersed droplets themselves enclose even more finely dispersed droplets of a separate phase. Thus, they may be Oil dispersed in Water dispersed in Oil (O/W/O) and Water dispersed in Oil dispersed in Water (W/O/W) multiple emulsions. More complicated multiple emulsions are also possible.

Emulsion phase separation process is imposed by thermodynamic rules, because as the oil and water form two continuous phases while they separate, the interfacial area of the dispersion and subsequently its free energy are reduced. Therefore, the properties of the emulsion (drop size distribution, mean drop size, viscosity, etc.) cannot remain invariables in time. In consequence, the stability of an emulsion is the capability of the dispersion to preserve its properties within a particular timeframe (Walstra, 2005). Most of petroleum emulsions that will be found in practice comprehend oil, water and surfactants, and exist in a metastable state that has high potential obstruction to inhibit coalescence of the dispersed phase.

Finally, the emulsion formation process is called emulsification and it can be completed by the action of devices such as turbine blenders, ultrasonic devices (Abismail et al., 1999), or by the flow of the two phases through a membrane (van der Graaf, Schroen and Boom, 2005) or static mixers (Berkman and Calabrese, 1988). Spontaneous emulsification can also occur when the phases are contacted and for example, by chemical reactions (Nishimi and Miller, 2001).

2.1.2 Surfactants

A surface-active agent, or surfactant, is a chemical substance whose molecules are amphiphilic, which means that a portion of them is hydrophilic (has affinity for water or aqueous phases) and the other portion is lipophilic (has affinity for oily or organic phases). This combination of antagonist affinities in the same molecule is the dual chemical nature that confers the surfactant a specific behavior when in solution. Figure 2.1 shows the graphic representation of a generic surfactant molecule.

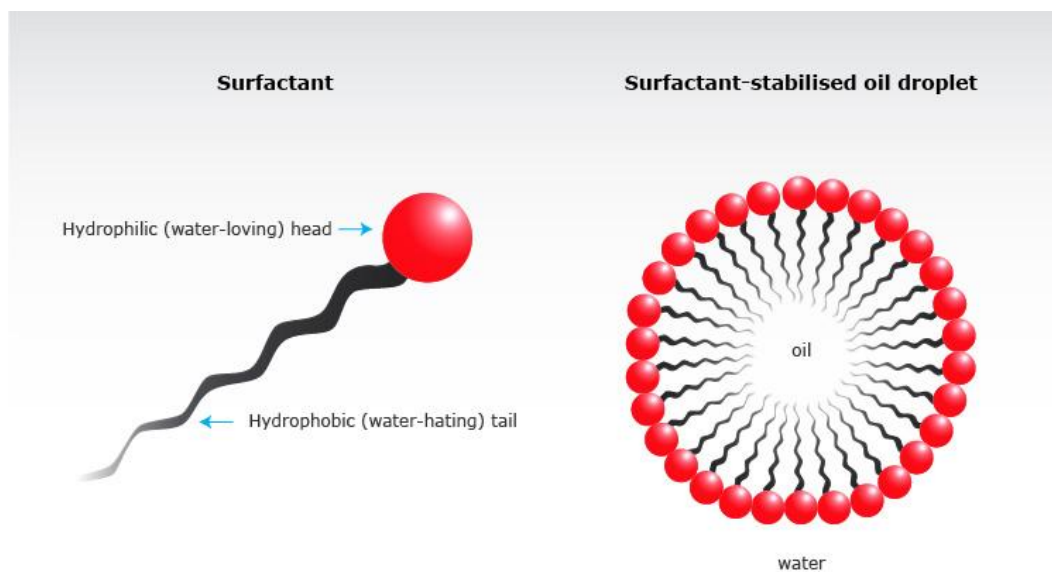


Figure 2. 1 Conventional representation of a generic surfactant molecule. (Copyright 2012. University of Waikato. All rights reserved. www.sciencelearn.gov.nz).

There are various classes of surfactants, depending on the nature of the hydrophilic and lipophilic chains. The lipophilic or hydrophobic group is usually a long chained highly branched hydrocarbon radical, normally in the range $C_8 - C_{20}$ (8 to 20 carbon atoms). These radicals frequently come from natural fatty acids, paraffins, olefins, or alcohols. Still, they may contain other structures such as alkyl benzenes, alkylnaphtalenes, partially or completely fluorinated fluorocarbons, polydimethylsiloxanes (silicone oil adducts), or high-molecular weight polyoxypropylene chains. The nature of the hydrophilic group can also be very diverse. In fact, the most common surfactant classification system is based on it. According to its nature, surfactants can be divided into ionic and nonionic, depending on whether or not they dissociate (ionize) in aqueous solution. Ionic surfactants can be further sub-classified into anionic and cationic.

2.1.2.1 Critical micelle concentration

When surfactant molecules are in aqueous solution, they tend to adsorb on the interface to minimize contact between their hydrophobic part and water, causing a decrease in the interfacial tension. The fact that the surfactant molecules gather at the interface means that the surface excess concentration is positive. Therefore, the reduction in interfacial tension increases as the surfactant concentration increases. However, at a certain concentration, the interface gets saturated and the surfactant molecules start self-assembling into aggregates called micelles. Micelles are spherical clusters of surfactant molecules with their hydrophobic groups directed towards the interior of the cluster and their hydrophilic part directed towards the water (Patist et al, 2002). The concentration at which this occurs is specific of each surfactant and is known as the Critical Micelle Concentration (CMC).

At concentrations higher than CMC, the interfacial tension remains almost constant. This occurs because the interface is completely covered with surfactant. Any new quantity of surfactant added after the CMC will either join the micelles or form new ones, changing the chemical potential of the solution, and keeping conditions at the interface almost constant (Nagarajan and Wang, 1996) . Figure 2.2 illustrates the behavior of surfactants at a liquid interface.

The interfacial tension is not the only property of the system that undergoes an abrupt change at the CMC. Other properties with strong changes include osmotic pressure, turbidity, and conductivity (ionic surfactants case). CMC values obtained by different methods fluctuate slightly, and the sharpness of the break in Figure 2.2.c depends on the surfactant nature. Therefore, the CMC should be regarded as a range of concentrations or an approximation.

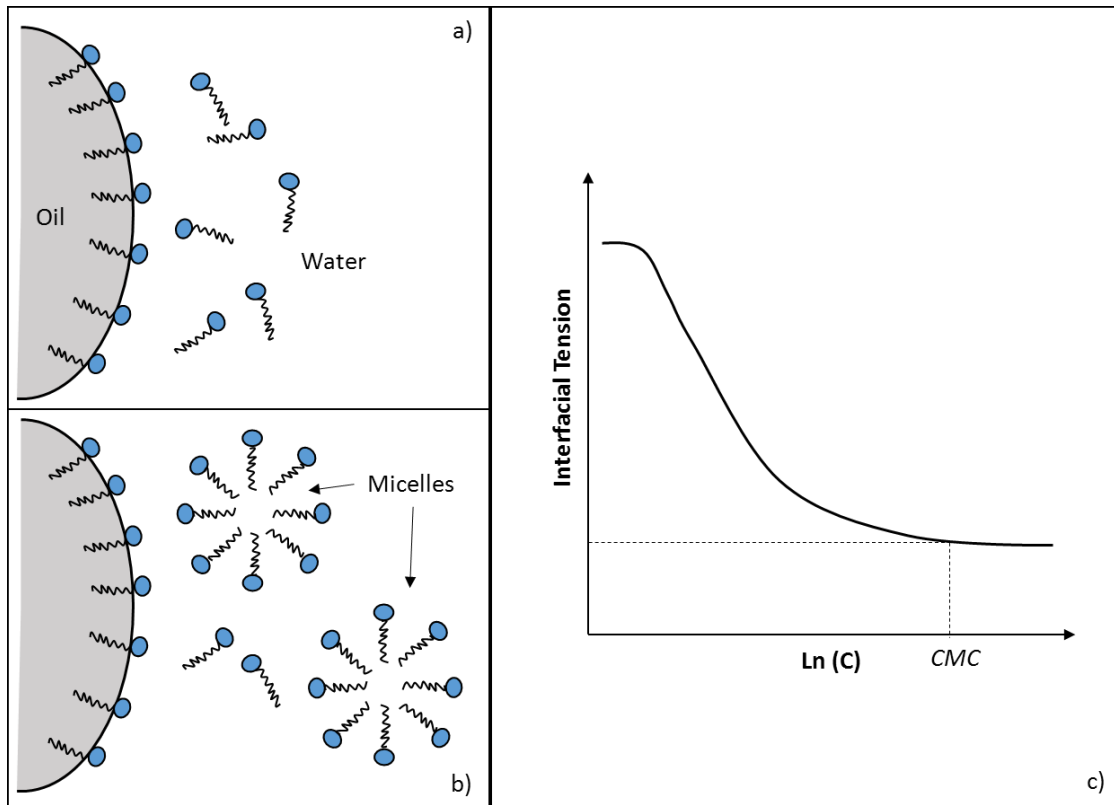


Figure 2. 2 Behavior of surfactants in a liquid-liquid system, a) concentration below the CMC; b) concentration above the CMC; c) curve equilibrium interfacial tension vs. logarithm of concentration for a typical surfactant.

2.1.3 Emulsion properties

2.1.3.1 Morphology of emulsions

The morphology, or spatial arrangement of the phases in an emulsion, defines its nature as W/O, O/W or multiple emulsions. Morphology is the simplest characteristic of an emulsion, and there are usually specific qualitative techniques that are used to discriminate each type of emulsion. They are based on the determination of the predominant polarity in the continuous phase, for example, contacting a drop of the emulsion dispersed phase with water or oil and observing its miscibility in each phase. However, results from such tests are sometimes ambiguous and do not allow to discern between simple and multiple emulsions. The morphologies of some different type of emulsions are shown in Figure 2.3.

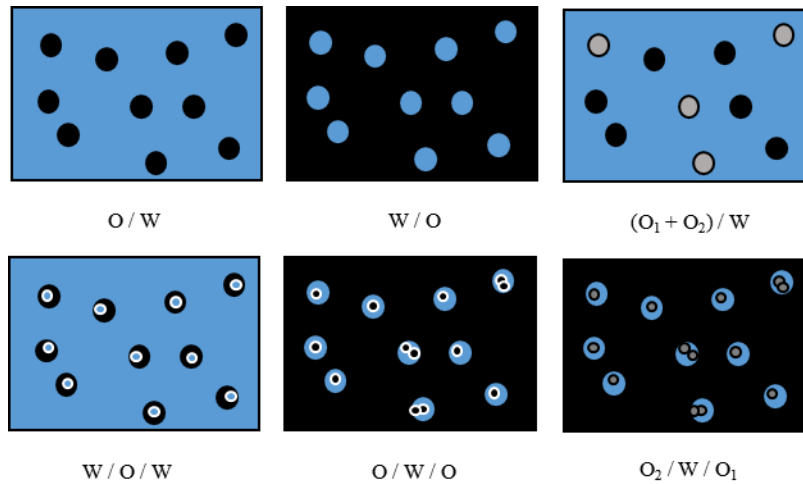


Figure 2. 3 Common morphologies of emulsions.

Electrical conductivity measurements are similarly used to define the type of emulsion. The water phase in an emulsion typically contains electrolytes and in most circumstances, non-polar fluids show very low electrical conductivity. As a result, the conductivity of an emulsion is high when water is the continuous phase and low when oil is the continuous phase (Salager et al., 1983). In addition, the optical microscopy method can also be used to discriminate between simple and multiple emulsions, because of the difference between the water and oil phase under observation.

2.1.3.2 Phase inversion

The phase inversion phenomenon is the process in which the dispersed and continuous phases of an emulsion invert, abruptly altering its form from O/W to W/O or vice versa. Phase inversion can be one of two types: transitional and/or catastrophic. The first one is produced by fluctuating factors:

- aqueous phase salinity,
- oil nature,
- surfactant nature or HLB (Hydrophilic Lipophilic Balance),
- alcohol type and concentration, and
- temperature, especially with nonionic surfactants.

The catastrophic inversion is produced by increasing the volume fraction of the dispersed phase. Catastrophic inversion usually take place when the internal

volume fraction surpasses some specific value, typically close to the limit of critical close packing (64% for random packing and 74% for ordered packing). Above this limit, droplets are compressed against each other and the interfaces are deformed causing the emulsion to adopt a foam-like structure. Arirachakaran et al. (1989) conducted an extensive study on oil-water flow in horizontal pipes for various viscosity values. They described the morphology of emulsion as function of water fraction as shown in Figure 2.4.

There are other important factors affecting the inversion process as the nature and concentration of the surfactants and physical influences such as temperature or the application of mechanical shear. The emulsification protocol characteristics, which indicate the way the emulsion is made or modified or how the formulation or composition are changed as a function of time or space, can also be considered to be among the factors that phase inversion depends on (Gong et al., 2006).

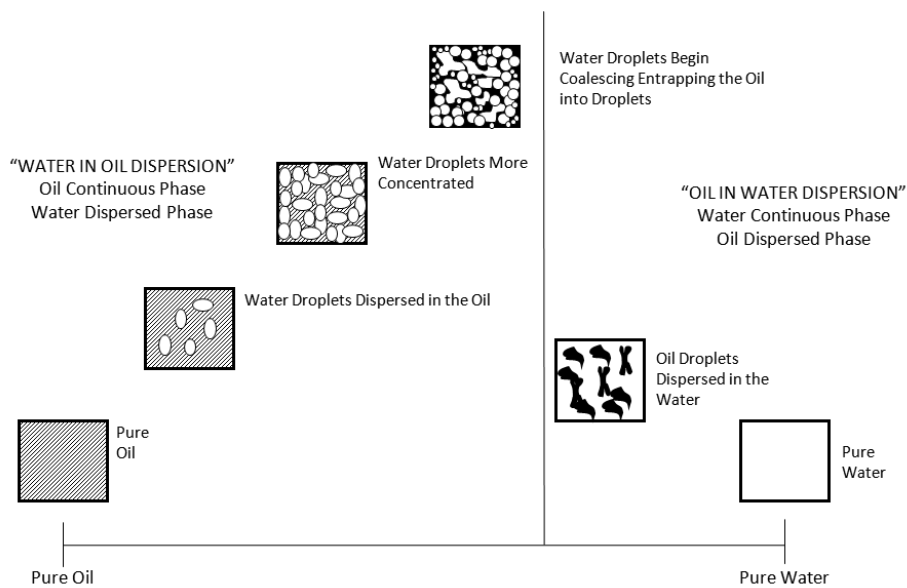


Figure 2. 4 Inversion process for oil-water dispersion flow. (Adapted from Arirachakaran et al., 1989)

2.1.3.3 Drop size distribution

The Drop Size Distribution (DSD) typically characterizes the structure of an emulsion. The knowledge of the DSD provides information on the efficiency of emulsification process, and the monitoring of any changes in the size distribution as the emulsion ages gives information on the stability of the system. Normally,

droplets in macro emulsions always exhibit finite polydispersity in their sizes, which usually range between 1 and 1000 μm . The resultant DSD is a statistical inventory of the dispersed phase. Valuable information is obtained from the DSD because the sizes of the droplets affect other properties of the emulsion such as its stability and rheology, subsequently the DSD can be understood as the fingerprint of the emulsion characterization.

Although the collection of particle sizes in an emulsion is discrete, the number of drops is typically large enough to permit describing its DSD with a continuous mathematical expression, ordinarily a Probability Distribution Function (PDF) (Kolmogorov, 1956). A commonly used form to determine the parameters of this PDF as an analytical expression is the lognormal function as defined in Equation 2.1 below. This appears to be a practical description of the droplet size distribution of many emulsions (Epstein, 1948 and Lachaise et al., 1995). Additionally, it has only two parameters, which make it convenient for modeling purposes (Lönnqvist et al., 1997).

$$PDF(a) = \frac{1}{2a\sigma_g\sqrt{2\pi}} \exp\left(-\frac{(\ln 2a - \ln d_0)^2}{2\sigma_g^2}\right) \quad (2.1)$$

Where a is the droplet radius, d_0 denotes the diameter median and σ_g is the geometric standard deviation of the DSD.

It must be pointed that there are several cases where the lognormal distribution does not fit the DSD and an additional distribution function must be assumed empirically. Figure 2.5 shows the drop size distributions that are usually found in emulsions.

The most universally reported characteristic of an emulsion is the mean drop size. Expressions for different types of average size are shown in Table 2.1. Two particularly relevant moment-based mean diameters are the d_{32} and the d_{43} . The d_{32} , also known as the Sauter mean diameter, is the surface-weighted mean diameter and it is frequently found in the spray, atomization, and liquid-liquid dispersion literature. One common approach to define the distribution width is to cite three values on the x-axis, the d_{10} , d_{50} , and d_{90} as shown in Figure 2.6. The d_{50} , the median, is defined as the diameter where half of the population lies below this value. Similarly, 90% of the distribution lies below the d_{90} , and 10% of the population lies below the d_{10} .

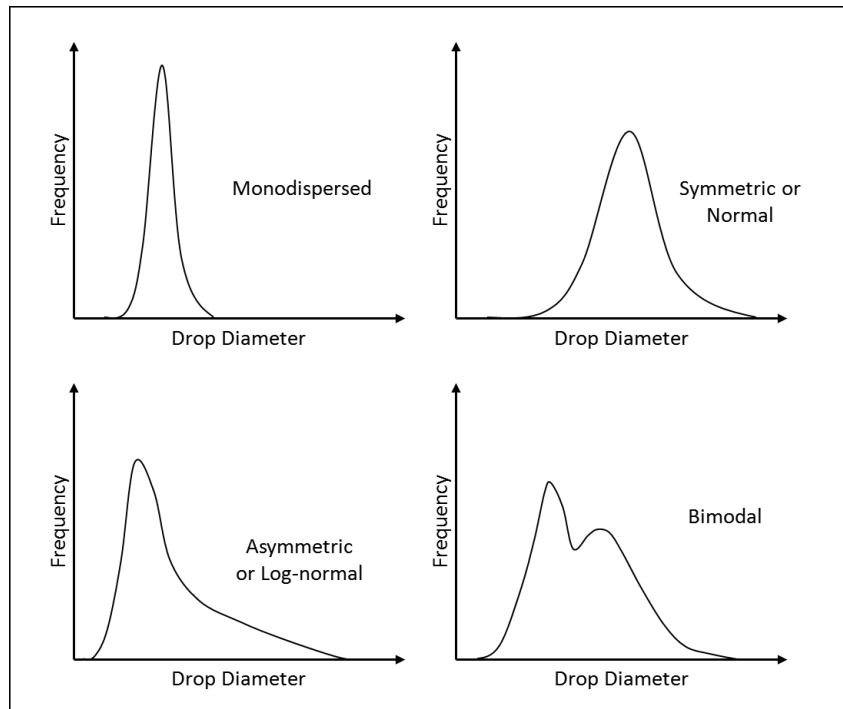


Figure 2. 5 Typical DSD in emulsions.

Table 2. 1 Mean drop sizes used to characterize emulsions.

| Descriptive Name | Symbol | Discrete Distribution |
|--|----------|--|
| Number – Length Mean (Arithmetic Mean) | d_{av} | $\frac{\sum d \Delta N}{\sum \Delta N}$ |
| Number – Surface Mean (Surface Mean) | d_s | $\left(\frac{\sum d^2 \Delta N}{\sum \Delta N}\right)^{1/2}$ |
| Number – Volume Mean (Volume Mean) | d_v | $\left(\frac{\sum d^3 \Delta N}{\sum \Delta N}\right)^{1/3}$ |
| Length – Surface Mean (Linear Mean) | d_{21} | $\frac{\sum d^2 \Delta N}{\sum d \Delta N}$ |
| Length – Volume Mean (Volume Diameter Mean) | d_{31} | $\left(\frac{\sum d^3 \Delta N}{\sum d \Delta N}\right)^{1/2}$ |
| Surface – Volume Mean (Sauter Mean Diameter) | d_{32} | $\frac{\sum d^3 \Delta N}{\sum d^2 \Delta N}$ |
| Volume – Moment Mean (De Brouckere Mean Size) | d_{43} | $\frac{\sum d^4 \Delta N}{\sum d^3 \Delta N}$ |

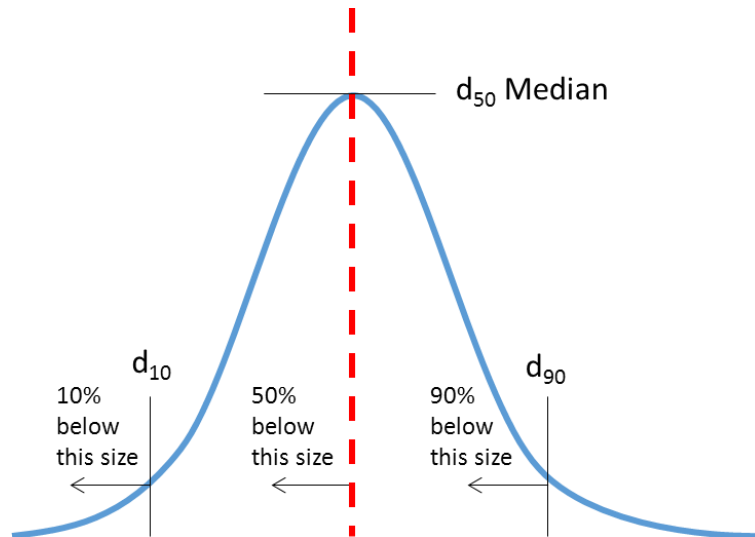


Figure 2. 6 Graphical definition of d_{10} , d_{50} and d_{90} in a DSD.

2.1.3.4 Emulsions stability

Emulsions are, by nature, systems thermodynamically unstable. They tend to separate into its initial (forming) phases over time due to the high interfacial area, for that reason, the emulsion characteristics (drop size distribution, mean drop size and other properties) will change with the time. The stability or instability of an emulsion is given by the time-dependent behavior of its basic parameters.

Many emulsion breakdown processes are identified. Some of these instability mechanisms that lead to phase separation are sedimentation and creaming, aggregation and coalescence, as represented in Figure 2.7. Gravitational separation or creaming takes place when the two liquids exhibit different densities. Aggregation occurs when droplets stay very close to one another for far longer time than if there were no attractive forces acting between them (Walstra, 2005). Coalescence takes place when the thin film of continuous phase between two drops breaks and they fuse rapidly to form a single droplet.

Figure 2.7 also shows mass-transfer processes that can take place in emulsions if at least one solute can be transferred across the continuous phase. If the concentration of solute in the external phase is below the saturation limit, solubilization takes place and drop sizes diminish. If the continuous phase is slightly supersaturated in the solute, Ostwald ripening occurs (Peña and Miller, 2006). In this case, large drops grow at the expense of those smaller because the

chemical potential of the solute is higher in drops with greater interfacial curvature. Emulsions with droplets of different composition may undergo compositional ripening, or exchange of matter due to differences in concentration between drops (Weiss, Cancelliere and McClements, 2000).

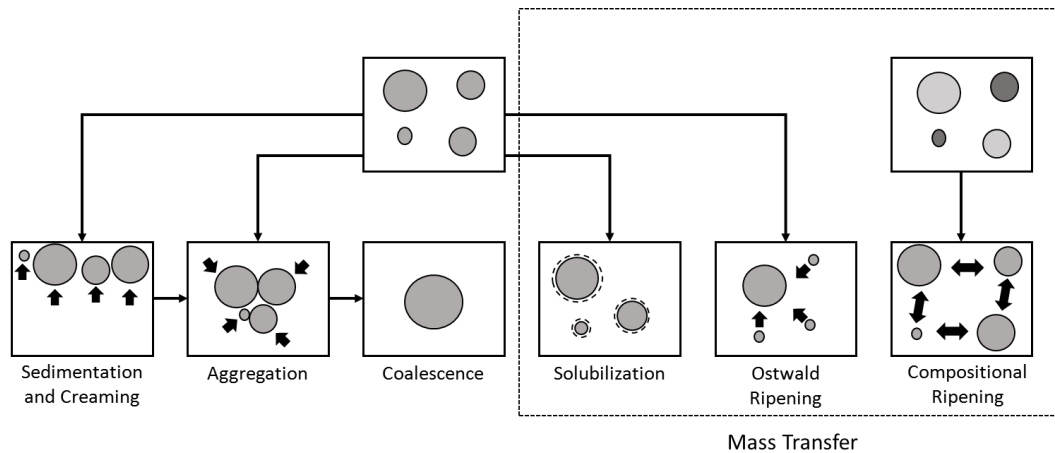


Figure 2. 7 Destabilizing mechanisms in emulsions.

2.2 Drop breakup in turbulent flow

In most of liquid-liquid dispersion common unit operations in chemical, petroleum and pharmaceutical industries (heat and mass transfer processes, polymerization reactor design, crude oil treatment, etc.), emulsion DSD is a very important parameter, because significantly affects the processes efficiency and/or final product's properties. Therefore, accurate models for prediction of the drop size are greatly desired. Various researchers have developed models for drop breakup in turbulent flows (Kolmogorov, 1949; Hinze, 1955; Shinnar and Church, 1960; among others), usually based on the theory of isotropic turbulence first proposed by A.N. Kolmogorov (1941). Many of these models are restricted to dilute, inviscid systems at equilibrium in stirred tanks. However, several investigations have been extended or modified to include the effect of higher dispersed phase concentration (Coulaloglou and Tavlarides 1976; Chatzi, Gavrielides and Kiparissides, 1989), the dispersed phase viscosity (Calabrese, Chang and Dang, 1986; Wang and Calabrese, 1986; Davies, 1987), and to predict transient drop sizes (Baladyga and Podgórska, 1998).

To familiarize with the fundamentals of drop breakup process in turbulent flow, a simple overview to the phenomenon of turbulence and some of its most basic concepts, as well as Kolmogorov's theory for the smaller scale turbulence properties will be introduced. Then, the development of mechanistic models for drop breakup in turbulent flows will be exposed. Finally, a brief discussion of the hydrodynamics of the turbulent flows cases considered in this dissertation will be provided.

2.2.1 Introduction to turbulent flow

Turbulence is a universal and important phenomenon; it appears in many diverse and apparently unrelated fields such as meteorology, astrophysics, and several engineering specialties.

There are certain characteristics that a flow must exhibit to be considered turbulent. The first one is randomness. Turbulent flows are time and space dependent with a very large number of degrees of freedom (Mathieu and Scott, 2000). Any amount of energy put into a frictionless (very low viscosity) fluid, be it liquid or gas, is immediately distributed among all degrees of freedom, which makes turbulence a statistical problem (Heisenberg, 1948). This random nature is demonstrated by quantitative determination of instantaneous velocities in turbulent flows, resulting in randomly fluctuating signals. Although randomness makes turbulence unpredictable, statistical tools and averages are used to describe it effectively. In addition to the statistical random background, there are coherent structures (e.g. vortices, jets and sweeps) present in most turbulent flows. These coherent structures are regular, well-defined sequences of events that may still be random about their occurrence in time and space (McDonough, 2007).

Another significant characteristic of turbulence is that it contains a wide range of coexisting space and time scales, with the smaller ones living inside larger ones (Mathieu and Scott, 2000). The larger scales are usually dictated by the global geometry of flow, while the smallest ones depend on the fluid's viscosity. The presence of these various scales is related to the third defining characteristic of turbulence, the fact that it dissipates energy. Kinetic energy is supplied to the flow by a large-scale source (a pump, for example), which creates

instabilities in the flow, generating large-scale eddies. These large-scale eddies are also unstable and they disintegrate, creating and transferring their energy to smaller eddies, which continue doing the same until the energy is ultimately dissipated (into heat) at the smallest scales by viscous stresses. If there is no energy supply to maintain the flow, the turbulence decays and eventually ceases (Mathieu and Scott, 2000). The continuous energy transfer from larger eddies to smaller eddies is usually referred to as the “energy cascade” and is represented by the flow’s energy spectrum, a plot that shows how the kinetic energy is distributed among the different scales of the flow (Kraichnan, 1971). There are other defining characteristics of turbulence, such as the fact that it is a continuum phenomenon (the smallest scales are orders of magnitude larger than the molecular mean free path), which means that it may be described by continuum based equations; and that it has small-scale random vorticity, and is therefore, intrinsically three-dimensional.

2.2.1.1 Reynolds decomposition

Because of the random nature of turbulence, it is easier to decompose the instantaneous velocity into a mean motion and a fluctuating motion:

$$U = \bar{U} + u \quad (2.2)$$

Where U is a fluid velocity component, \bar{U} is its mean value, and u is the fluctuating velocity. This variable decomposition is known as Reynolds decomposition. The mean velocity \bar{U} is the result of some kind of averaging. There are different forms of averages used in turbulent flow analysis:

- ensemble average: average of the velocity component, at the same point in space and time, over several independent realizations of the flow field;
- spatial average: average of values at different points on a plane, at the same time;
- temporal average: average of values at the same location over a sufficiently long period.

The latter is the most commonly used, and is given by:

$$\bar{U}(\vec{x}, t) = \frac{1}{T} \int_{t-(T/2)}^{t+(T/2)} \bar{U}(\vec{x}, \xi) d\xi \quad (2.3)$$

Where \vec{x} the position vector in space is, t is time, and T is the period over which the average is taken. Figure 2.8 shows the decomposition of an instantaneous velocity component into its time-averaged mean component and fluctuating component.

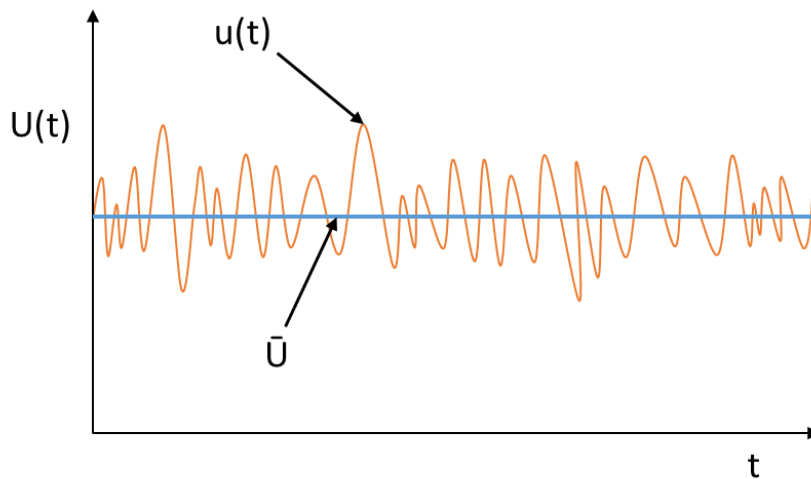


Figure 2. 8 Decomposition of the instantaneous velocity component U into a mean component (\bar{U}) and a fluctuating component (u).

Applying Reynolds decomposition (Equation 2.2) to the kinetic energy transport equation, the following expression is obtained:

$$\frac{\partial K}{\partial t} + \bar{U}_j \frac{\partial K}{\partial x_j} = -\bar{u}_i \bar{u}_j \frac{\partial \bar{U}}{\partial x_i} - \varepsilon - \frac{1}{\rho} \frac{\partial \bar{p} u_i}{\partial x_i} + \nu \nabla^2 K - \frac{\partial u_j (u_i^2/2)}{\partial x_j} \quad (2.4)$$

Where K is the turbulent kinetic energy ($K = 1/2 \overline{u_i^2}$) per unit mass, p is the pressure fluctuation, ν is the fluid's kinematic viscosity, and ε is the turbulent energy dissipation rate per unit mass, defined as:

$$\varepsilon = \nu \overline{\left(\frac{\partial u_i}{\partial x_j} \right)^2} \quad (2.5)$$

The physical interpretation of equation 2.4 is that the rate of change of turbulent kinetic energy in the control volume, plus the net rate of gain or loss by

convection through the boundaries, is balanced by the rate of turbulent kinetic energy production, the rate of turbulent kinetic energy dissipation, the pressure work, and the viscous and turbulent diffusion through the control volume surface, which are only significant near boundaries (Pope, 2000). The turbulent energy dissipation rate is always positive (Equation 2.5), and therefore acts as an energy sink caused by friction (viscous forces). Of all the terms in the energy balance equation, ε is the most difficult to measure or calculate accurately, however, it is one of the most important quantities in turbulent flow analysis.

2.2.1.2 Isotropic turbulence

The term isotropic turbulence is used to denote a turbulent flow field in which the statistical properties are independent of the position and orientation of the coordinate axes; that is to say, symmetric with respect to any plane or rotation (Mathieu and Scott, 2000). Isotropy must not to be confused with homogeneity. In homogeneous turbulence, the fluctuation statistics are the same in all spatial positions, and yet, the mean flow may be non-uniform (Mathieu and Scott, 2000). Isotropy implies homogeneity, but the opposite is not true since some flows may be homogeneous in one direction and not in the others, which is incompatible with the symmetry requirements for isotropy. One of the consequences of the symmetries of isotropy is that the mean flow must be constant (all mean flow gradients are equal to zero). In addition, the mean fluctuating velocity is the same in all directions:

$$\overline{u_1^2} = \overline{u_2^2} = \overline{u_3^2} = u'^2 \quad (2.6)$$

Where u' is also known as the Root Mean Squared (RMS) velocity difference. Additionally, under isotropic conditions, the turbulent kinetic energy equation (Equation 2.4) reduces to,

$$\frac{\partial K}{\partial t} = -\varepsilon \quad (2.7)$$

This shows that isotropic turbulence is unsteady and decaying. G.I Taylor (1935), showed that for the case of incompressible isotropic turbulence:

$$\varepsilon = 15\nu \overline{\left(\frac{\partial u_1}{\partial x_1}\right)^2} = \frac{15}{2}\nu \overline{\left(\frac{\partial u_1}{\partial x_2}\right)^2} \quad (2.8)$$

Where $\partial u_1/\partial x_1$ is the gradient of a fluctuating velocity component in the parallel direction to it and $\partial u_1/\partial x_2$ is the gradient in one of the perpendicular directions. This simplifies to a great extent turbulence experiments and modeling, since only one fluctuating velocity gradient needs be measured or predicted to calculate ε .

2.2.1.3 Local isotropy

Isotropic turbulence at all scales is almost impossible to achieve by means other than forced experiments or numerical simulation. It has little applicability in engineering. In 1941, A.N. Kolmogorov introduced the concept of local isotropy. Turbulent flows normally have high values of Reynolds number, which is defined as:

$$Re = \frac{LU}{\nu} \quad (2.9)$$

Where L and U are the typical length and velocity for the whole flow, respectively. Kolmogorov postulated that, if the Reynolds number is sufficiently high, it is very likely that there will be a small spatial domain, with linear dimensions smaller than L and not near any boundaries or flow singularities, in which the flow could be considered isotropic. Furthermore, Kolmogorov predicted that in locally isotropic turbulence the statistical characteristics of the flow only depend on the turbulent energy dissipation rate (ε) and the fluid's kinematic viscosity (ν), and that the length and time scales of the smallest eddies in the flow, the ones that dissipate energy into heat, are given by:

$$\lambda_K = \left(\frac{\nu^3}{\varepsilon}\right)^{1/4} \quad (2.10)$$

$$\tau_n = \sqrt{\frac{\nu}{\varepsilon}} \quad (2.11)$$

Where, λ_K is the length scale and τ_n is the time scale. However, for eddies that are larger than λ_K , but still very small compared to L , the flow is independent of viscosity and uniquely determined by ε .

Kolmogorov's theory revolutionized the study of turbulence since it gives the character of a universal equilibrium to the smallest scales of the flow, in which statistical and structural properties are common to all turbulent flows (Pope, 2000) independently of their macro-scale geometry. One consequence of local isotropy is the existence of the "inertial sub-range", the range of small scales (smaller than L and larger than λ_K) that are characterized exclusively by ε . Kolmogorov determined, from dimensional analysis, that in this range, the energy spectrum depends only on ε and the wavenumber (k) of eddies (the inverse of the apparent eddy length):

$$E(k, t) = C_K k^{-5/3} \varepsilon^{2/3} \quad (2.12)$$

Where E is the energy spectral density function and C_K is the Kolmogorov constant. In this range of the spectrum, inertial forces predominate over viscous forces, that is why the name of "inertial sub-range".

The range of wavenumbers greater than λ_K^{-1} (length scales smaller than λ_K) is called the "viscous sub-range", since here is where the viscous dissipation of energy takes place. Heisenberg (1948) obtained that $E(k) \sim k^{-7}$ in this wavenumber range, therefore, the expression for the energy spectral density function is (Chen and Middleman, 1967):

$$E(k) = \left(\frac{\alpha \varepsilon}{2\nu^2} \right)^2 k^{-7} \quad (2.13)$$

According to equation 2.13, the functional dependence of $E(k)$ on k shifts from the Kolmogorov predicted exponent of $-5/3$ to -7 , indicating the dissipative effect of the viscosity at these scales. Figure 2.9 shows a schematic representation of a typical energy spectrum with all the ranges specified.

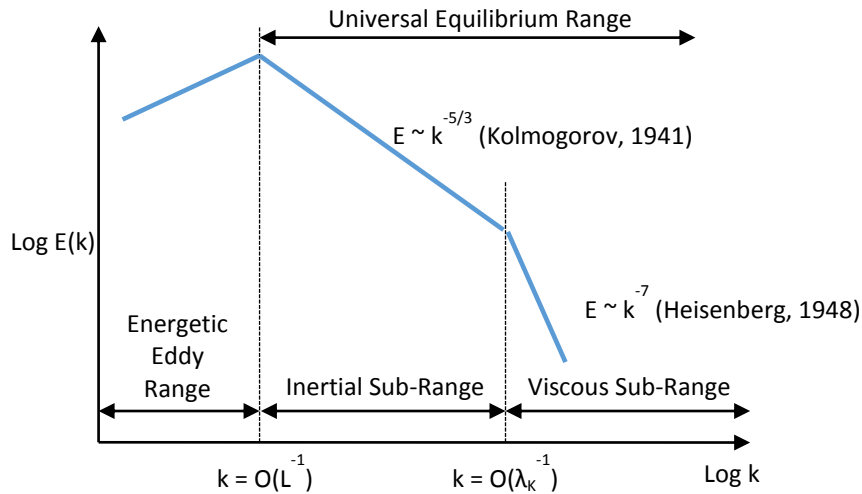


Figure 2. 9 Schematic representation of the energy spectrum of a turbulent flow.

2.2.2

Mechanistic model for drop breakup in turbulent flow

Many theoretical and empirical models have been developed to predict and analyze drop breakup and coalescence in turbulent flows. In the case of dilute systems (dispersions with very low dispersed phase content), coalescence may be neglected, and the breakup models are based on a balance of the disruptive and cohesive forces acting on a drop in an isotropic turbulent flow field. If the drop is considered viscous ($\mu_d > \mu_c$, where μ_d is the dispersed phase viscosity and μ_c the continuous phase viscosity), the cohesive forces that oppose the deformation of the drop are those due to the interfacial tension and those due to the dispersed phase viscosity. The cohesive forces due to the interfacial tension try to keep the drop's spherical form; meanwhile the forces due to the dispersed phase viscosity increase the resistance of the intern drop fluid to flow, delaying the deformation. The disruptive forces are those exerted by the continuous phase on the drop. In the case of a small drop ($L \gg d$, d being the drop's diameter) in a turbulent flow, these forces are isotropic (no matter how complex the geometry is) and may be inertial or viscous in nature, depending on whether the drop is in the inertial or the viscous sub-range.

Previous experimental studies (Calabrese et al., 2000 and van der Zande, Muntinga and van der Broek, 1998) have proved that in the cases of turbulent drop breakup of oil in water systems in the geometries considered in this dissertation (Rotor – Stator mixers and flow through an orifice in a pipe), the size of the maximum stable drops tends to be higher than the Kolmogorov's length

micro-scale λ_K , but smaller than the flow's characteristic length L . Therefore, it can be assumed that stable droplet sizes will be in the inertial sub-range.

2.2.2.1 Mechanistic model for the inertial sub-range

In the inertial sub-range ($L \gg d \gg \lambda_K$), the energy of the continuous phase is described by the energy spectral density function of Equation 2.12. The principal mechanistic model used to describe the drop breakup process in the inertial sub-range is the linear model, which is based on the balance of cohesive and disruptive forces acting on the droplet.

2.2.2.1.1 Linear model

As previously stated, this model is based on a simple balance between disruptive and cohesive forces, which act on the droplet. The disruptive force per unit area or turbulent stress acting on a drop of diameter d is given by:

$$\tau_c = \rho_c u'^2(d) \quad (2.14)$$

Where $u'(d)$, the RMS velocity difference is the mean velocity difference between two points in the continuous phase separated by a distance equal to d . In other words, the stress acting on the drop is equal to the dynamic pressure difference between its opposite sides (Walstra, 1993).

From Kolmogorov's theory (Kolmogorov, 1941), the RMS velocity difference is related to the energy spectrum as expressed by Equation 2.15.

$$u'^2(d) = \int_{1/d}^{\infty} E(k) dk \quad (2.15)$$

Meaning that only the energy contained in eddies of size equal to or smaller than the drop ($k = 1/d - \infty$) are considered, since larger eddies only carry the drop rather than deform it (Paul, Atiemo-Obeng and Kresta, 2004). Subsequently, from Equations 2.12, 2.14 and 2.15, the expression for the stress (force per unit area) exerted by the turbulence of the continuous phase on the deforming drop is:

$$\tau_c \sim \rho_c \varepsilon^{2/3} d^{2/3} \quad (2.16)$$

The surface energy of a drop is proportional to the interfacial tension between the dispersed and continuous phases. When the drop is deformed, its surface area and surface energy increase. Such energy increase is thermodynamically unfavorable and, as a result, the higher the increase in surface area, the higher the force that opposes the drop deformation. In other words, smaller drops have a higher internal pressure according to the Young-Laplace equation (Finn, 1999), and hence, are more difficult to deform. Consequently, the interfacial stress that opposes the drop deformation scales with drop size is:

$$\tau_s \sim \frac{\sigma}{d} \quad (2.17)$$

Where τ_s is the interfacial stress and σ is the interfacial tension.

The deformation of the drop's interface by the turbulent forces of continuous phase gives rise to viscous stresses inside the drop. According to Hinze (1955), the flow velocity inside the drop is proportional to $(\tau_c/\rho_d)^{1/2}$. Therefore, applying Newton's law of viscosity, the viscous stresses that oppose the drop's deformation are estimated by:

$$\tau_d \sim \frac{\mu_d}{d} \left(\frac{\tau_c}{\rho_d} \right)^{1/2} \quad (2.18)$$

The maximum stable drop diameter in the dispersion (d_m) is that for which the disruptive and cohesive forces are at equilibrium (Wang and Calabrese, 1986):

$$\tau_c(d_m) = \tau_s(d_m) + \tau_d(d_m) \quad (2.19)$$

By substituting equations 2.16, 2.17 and 2.18 into equation 2.19, the following expression is obtained:

$$\rho_c \varepsilon^{2/3} d_m^{2/3} = C_1 \frac{\sigma}{d_m} + C_2 \frac{\mu_d}{d_m} \sqrt{\frac{\rho_c \varepsilon^{2/3} d_m^{2/3}}{\rho_d}} \quad (2.20)$$

Where C_1 and C_2 are arbitrary constants of proportionality (from now on C_n , where n is an integer, will be used to designate proportionality constants).

Rearranging the previous equation and solving for d_m :

$$d_m = C_3 \left(\frac{\sigma}{\rho_c} \right)^{3/5} \varepsilon^{-2/5} \left[1 + C_4 \frac{\mu_d}{\sigma} \sqrt{\frac{\rho_c}{\rho_d}} \varepsilon^{1/3} d_m^{1/3} \right]^{3/5} \quad (2.21)$$

Equation 2.21 is the representation of the mechanistic model for the maximum stable size of viscous drops that breakup in:

- dilute dispersions,
- the turbulent inertial sub-range and in
- clean systems (surfactant free).

The presence of surfactants in liquid–liquid systems generates some physicochemical singularities (surfactant adsorption dynamics, interfacial rheology, Marangoni effects, etc.) which affect the drop – drop interactions, decreasing (in most cases) the equilibrium mean drop diameter (Koshy, Das and Kumar, 1988; Chatzi, Boutris and Kiparissides, 1991; Lucassen-Reynders and Kuijpers, 1992). Nevertheless, Tcholakova, Denkov and Danner (2004) showed that for a defined surfactant-rich regime (surfactant concentration higher than 0.1% wt.), the mean drop diameter does not depend on surfactant concentration and is determined by the interfacial tension and by energy dissipation rate in the system. They also concluded that the measured values of mean drop sizes are described very well by the Kolmogorov – Hinze theory of emulsification for all studied systems. Thus, despite the presence of surfactant in the emulsions used in this investigation, the results obtained by Tcholakova, Denkov and Danner (2004) allow to use Equation 2.21 to describe the turbulent breakup of the systems studied in this dissertation.

Equation 2.21, however, is difficult to use directly, primarily because of the difficulty in obtaining exact values for ε . In stirred tanks and rotor – stator mixers, the turbulent energy dissipation rate, varies spatially, being higher near the mixing head than in the bulk of the fluid (Utomo, 2008). The equilibrium DSD will not be achieved until all drops have passed through the high-energy dissipation zones, which are where ε , and consequently drop deformation, reaches its maximum. For that reason, the value of ε used in equation 2.21 should be the maximum energy

dissipation rate value ε_m . Unfortunately, the exact value of ε_m is difficult to measure or predict.

In geometrically similar systems (Kolmogorov's first similarity hypothesis states that in every turbulent flow at sufficiently high Reynolds number, the statistics of the small scale motions have a universal form that is uniquely determined by ε and ν), the energy dissipation rate is proportional to the average dissipation rate, $\bar{\varepsilon}$ (Chen and Middleman, 1967). Thus the maximum stable drop size may be calculated as:

$$d_m = C_3 \left(\frac{\sigma}{\rho_c} \right)^{\frac{3}{5}} \bar{\varepsilon}^{-\frac{2}{5}} \left[1 + C_4 \frac{\mu_d}{\sigma} \sqrt{\frac{\rho_c}{\rho_d}} \bar{\varepsilon}^{\frac{1}{3}} d_m^{\frac{1}{3}} \right]^{\frac{3}{5}} \quad (2.22)$$

Depending of the proper definition for $\bar{\varepsilon}$, expressions derived from Equation 2.22 can be obtained as a function of a particular process and/or geometry and flow conditions.

2.2.2.1.1.1

Linear model for turbulent breakup in a rotor – stator mixer

In this case, the average energy dissipation rate can be approximated as the general expression of power draw per unit mass used for stirred tank contactors (Wang and Calabrese, 1986):

$$\bar{\varepsilon} = C_5 \frac{P}{\rho_c V} \quad (2.23)$$

The power draw (P) is equal to $P_0 \rho_c N^3 L^5$ (Padron, 2001), where P_0 is the power number, N is the impeller's rotational speed, and L is the characteristic length scale of the system, which for stirred tanks and rotor – stator mixers is the impeller or rotor diameter. For high Reynolds number ($Re > 10000$), which is already a requirement to apply local isotropy theory, the Power number is constant. Since the volume of the fluid in the tank is proportional to L^3 , the following expression is obtained:

$$\bar{\varepsilon} = C_6 N^3 L^2 \quad (2.24)$$

In the case of toothed rotor – stator mixers (as used in this work) with tip velocity v_T and tooth spacing of a_T , Brocart et al. (2002) proposed an expression to calculate the average energy dissipation rate per unit mass as:

$$\bar{\varepsilon} = \frac{v_T^3}{4a_T} = \frac{(\pi LN)^3}{4a_T} \quad (2.25)$$

From dimensional analysis, it is possible to note that Equations 2.24 and 2.25 are dimensionally equivalent. Therefore, Equation 2.25 will be used to quantify the energy dissipation rate per unit mass in the rotor – stator mixer case.

2.2.2.1.1.2

Linear model for turbulent breakup through an orifice

In this case, the energy dissipation is induced by the large velocity gradients that are present downstream of the orifice (See section 2.2.3.2). Turbulent flow extracts energy from the mean flow in regions where velocity gradients are present. By applying the conservation laws in integral form to a suitable control volume, it can be derived that in a duct flow the energy dissipation rate is equal to the pressure drop across the control volume times the flow rate through it (Kundu, Cohen and Dowling, 2012). In the case the control volume is defined around a restriction, the energy dissipation rate, \dot{E} in flow through the orifice is given by:

$$\dot{E} = \Delta p_{perm} Q \quad (2.26)$$

Where Δp_{perm} is the permanent pressure drop through the orifice and Q is the flow rate. The volume of the dissipation zone can be approximated to $A_0 L_{dis}$, where A_0 is the cross sectional area of the orifice and L_{dis} is the axial length of the dissipation zone. The mass of fluid in the dissipation zone is $\rho_c A_0 L_{dis}$. Therefore, from Equation 2.26, the mean energy dissipation rate per unit mass $\bar{\varepsilon}$ in the dissipation zone of the orifice is given by:

$$\bar{\varepsilon} = \frac{\dot{E}}{\rho_c A_0 L_{dis}} = \frac{\Delta p_{perm} U_0}{\rho_c L_{dis}} \quad (2.27)$$

Morrison et al. (1993) and van der Zande et al. (1999) have demonstrated that the axial length of dissipation is proportional to the pipe diameter D_p . In

addition, the dissipation length can be estimated from visualization of a region where there is no noticeable shear stresses acting on the droplets. Therefore, after the determination of dissipation length, Equation 2.27 will be used to quantify the energy dissipation rate per unit mass for the case of flow through an orifice.

2.2.3

Hydrodynamics of drop breakup in turbulent flow

Even with the practical existence of mechanistic models to predict the maximum stable drop size of oil and water biphasic systems (O/W emulsions in this case), there is still a lot of necessary information to define the real nature of drop breakup. The location of high-energy dissipation zones and the explanation of drop breakup mechanisms are, for example, part of the additional information required to make a better description of those systems. This section includes a literature review about computational simulations and visualizations concerning the drop breakup process in the two geometries considered in this dissertation.

2.2.3.1

Hydrodynamics of drop breakup in rotor – stator mixers

Rotor – stator mixers (RSM) are characterized by high-speed rotors surrounded closely by stators (Figure 2.10). The rotors rotate at speeds that are an order of magnitude higher than impellers in stirred tanks with typical tip speeds range from 10 to 50 m/s (Paul, Atiemo-Obeng and Kresta, 2004), while the gaps between the rotors and stators vary from 100 to 3000 μm (Karbstein and Schubert, 1995). They can generate high shear rate in the gap ranging from 20,000 to 100,000 s^{-1} (Paul, Atiemo-Obeng and Kresta, 2004) and therefore they are usually called High Shear Mixers (HSM). RSM also generate high intensity of turbulence. High kinetic energy supplied by the rotor dissipates mainly inside the stator and therefore the local energy dissipation rate in a rotor-stator mixer can be three orders of magnitude higher than in a conventional stirred vessel (Paul, Atiemo-Obeng and Kresta, 2004).

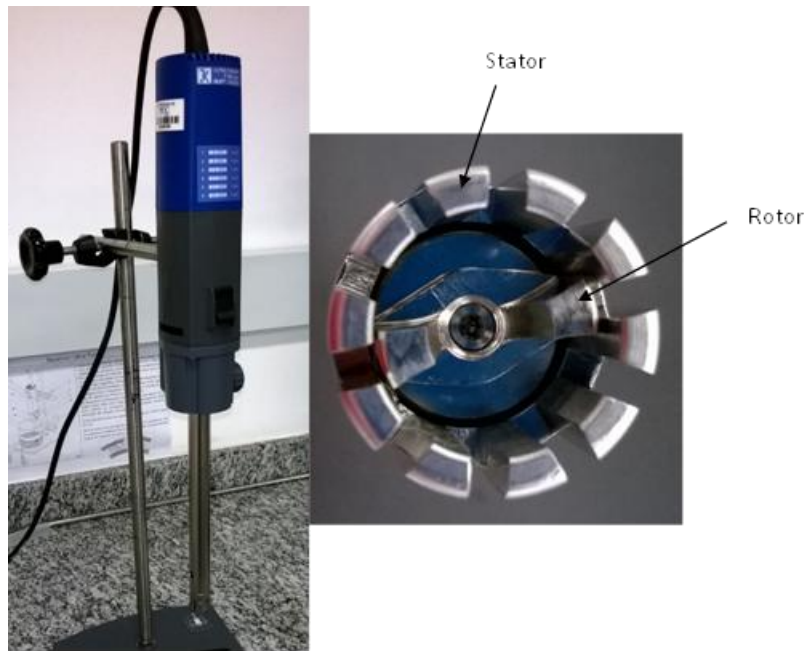


Figure 2.10 IKA T25 Basic RSM.

According to Paul, Atiemo-Obeng and Kresta (2004), RSM can be classified into colloid mills and toothed devices (Figure 2.11), axial discharge RSM where the rotors are axial impellers (Figure 2.12) and radial discharge RSM where the rotors are radial impellers (Figure 2.13). Colloid mills usually operate as in-line mixers with external pumps due to their limited pumping ability while axial and radial discharge RSM can operate as batch or in-line mixers, since they have a considerably pumping ability although significantly lower than open impellers (Myers, Reeder and Ryan, 2001).

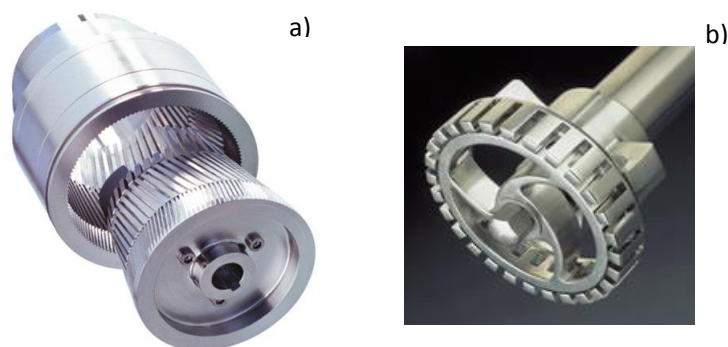


Figure 2.11 a) Colloid mill. b) toothed device



Figure 2. 12 Axial discharge RSM Greerco XLR homomixer.



Figure 2. 13 Radial discharge RSM Silverson L4RT.

In RSM, droplets can be disrupted by laminar shears, turbulent eddies, mechanical impact on the stator surfaces or combination of those factors (Myers et al., 2001).

In colloid mill, droplets are disrupted by laminar shear forces when the surfaces of rotor and stators are smooth and by turbulence when the surfaces are roughened or toothed. In a radial discharge RSM, Calabrese et al. (2000) showed that shear in the gap was not the predominant droplets breakage mechanism for turbulent regime. They also suggested that in the turbulent regime, droplets breakup by impingement on the stator surfaces and turbulent eddies in the jets emanating from stator slots.

Doucet, Ascanio and Tanguy (2005) experimentally studied the behavior of viscous fluids in batch RSM based on a rotor-stator assembly manufactured by VMI-Rayneri and consisting of a four-bladed impeller and slotted stator head, separated by a 1.5 mm shear gap. Both Newtonian and non-Newtonian fluids were

examined. They focused on visualizing and quantifying hydrodynamic properties in the laminar and transition regimes. The Newtonian portion of the work of Doucet et al. was extended with transient 3D Computational Fluid Dynamics (CFD) simulations by Barailler, Heniche and Tanguy (2006). In this study, the shear gap was 1.04 mm in width. Using POLY3D (enhanced with in-house features), torques, shear stresses, flow rates, and velocity fields were predicted for a number of low rpm laminar cases. The shear stress was quantified as a function of rotor angle. It was found that the maximum shear stress, located at the rotor tip, agreed closely with the nominal shear stress.

Pacek, Baker and Utomo (2007) studied a Silverson L4RT RSM with a standard disintegrating head in an unbaffled tank using both FLUENT and Laser Doppler Anemometry (LDA). The width of the shear gap was 0.175 mm, and the rotor speed was between 2000 and 4000 rpm. The FLUENT simulation was a 3D model with sliding mesh interface. They examined the velocities and turbulence dissipation rates, and found that the radial velocity of the jets and the flow through the stator slots are proportional to rotor speed. LDA velocity measurements generally agree with the CFD predictions. For both rotor speeds, it was found that 50% of the total energy dissipation occurred within the swept area of the rotor, and only 7.5% was dissipated at the leading edge of the stator holes. For the 2000 rpm case, 5.4% of the energy dissipation occurs in the shear gap, while for the 4000 rpm case, the shear gap is responsible for 10.8% of the energy dissipation rate. Instantaneously, the greatest energy dissipation does occur at the leading edge of the stator holes, but only periodically when the rotor blade is closing with the leading edges.

The effect of stator geometry on flow patterns and energy dissipation rates was studied by Utomo, Baker and Pacek (2009). Using the Reynolds Averaged Navier Stokes (RANS) equations, standard $k-\epsilon$ model, and enhanced wall functions, the flow in a Silverson L4RT RSM with three stator geometries (disintegrating head, slotted head, and square hole head as given in Figure 2.14) was analyzed using FLUENT. The flow pattern in the stator holes was analogous for all shapes and sizes of the holes with jets emerging in the proximity of the leading edges and circulation flow behind the jets (Figure 2.15).

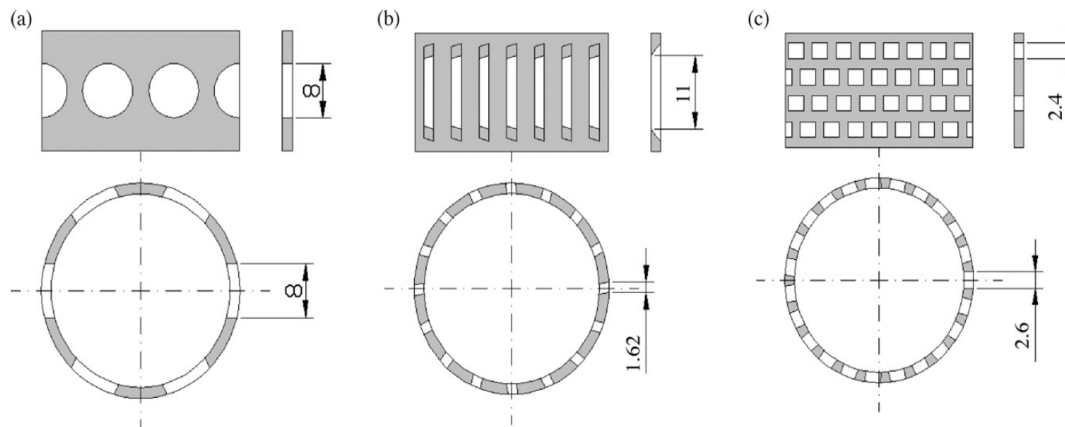


Figure 2. 14 Stator geometries considered in the Utomo, Baker and Pacek (2009) work. (a) disintegrating head, (b) slotted head, and (c) squared hole head. (Taken from Utomo, Baker and Pacek, 2009).

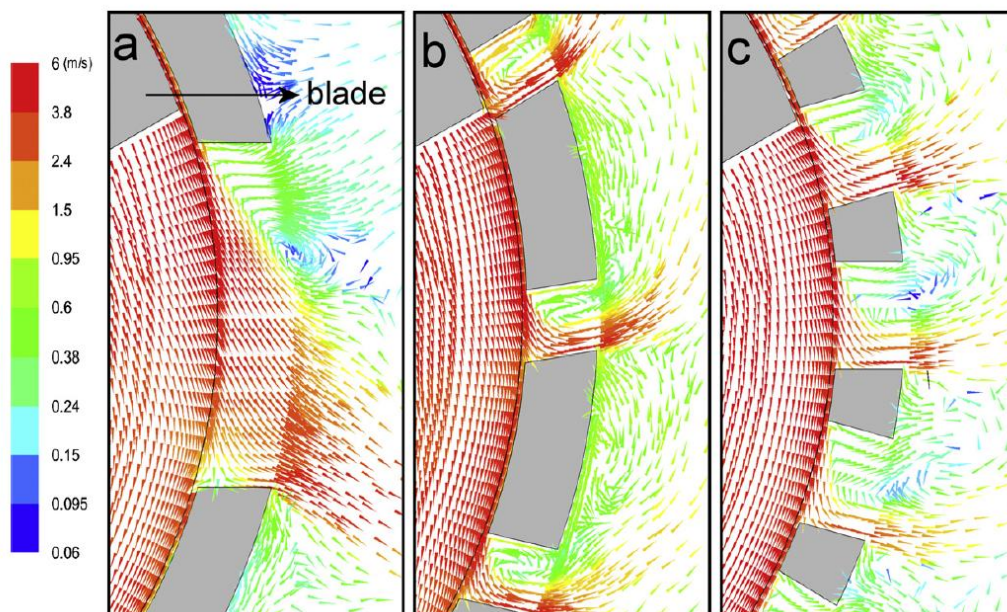


Figure 2. 15 Flow patterns (radial and tangential velocities) of the jets emerging from different stators: (a) disintegrating head, (b) slotted head and (c) squared hole head. (Taken from Utomo, Baker and Pacek, 2009).

Utomo, Baker and Pacek also indicated that larger holes resulted in longer jets. As holes became narrower, the circulation loops bent the jets and the energy dissipation rate became uniform. It was also shown that power number was proportional to flow rate, which was proportional to the cross-sectional area of the stator holes. Predicted power numbers were approximately 10% and 20% lower than experimental values for hole head (disintegrating and square) and slotted

head, respectively. The energy dissipated in the rotor swept region (about 50–60% of the total energy input) and in the jet region (about 25% of the total energy input) depends linearly of the flow rate, while the energy dissipated in the holes correlated better with the total surface area of the leading and trailing edges where the stagnation occurs.

2.2.3.2

Hydrodynamics of drop breakup through an orifice in a pipe

Flow through a circular orifice in a pipe exhibits the same characteristics as flow through an orifice plate, device used to measure the flow rate, either volumetric or mass flow (van der Zande, 2000). In Figure 2.16, these characteristics are schematically shown. The following description is valid for values of Reynolds number higher than 4000, although under special conditions, similar flow patterns have also been observed for lower values of the Reynolds number (Johansen, 1930). As the flow approaches the orifice, the fluid accelerates. Upstream of the orifice, a small recirculation zone develops. In the orifice, a high velocity jet is formed. Due to the inward motion of the fluid upstream of the orifice, the jet contracts to a diameter smaller than the orifice diameter. The point of minimum diameter is reached at a short distance downstream of the orifice and is called the vena contracta (vc). Close to the wall a large recirculation zone is formed. Due to the velocity gradient between the jet and the recirculation zone, turbulence is generated. Downstream of the vena contracta the jet starts to spread as surrounding fluid is entrained to the jet. At sufficient distance downstream of the restriction, the flow reattaches to the wall and the turbulent pipe flow redevelops.

When we focus on the pressure, the following description is valid. Upstream of the orifice, a high pressure is present. As the fluid approaches to the orifice, the velocity increases and, consequently, the pressure decreases. The position of minimum pressure does not necessarily coincide with the position of highest velocity. In general, however, it can be assumed that the minimum pressure is reached at the vena contracta. Here, the maximum pressure drop Δp_{max} is obtained. As the fluid decelerates downstream of the vena contracta, the pressure increases. The upstream pressure, however, will not be fully recovered. This is

due to the turbulent energy dissipation in the high velocity zone of the jet, downstream of the orifice. Consequently, a permanent pressure drop Δp_{perm} is present.

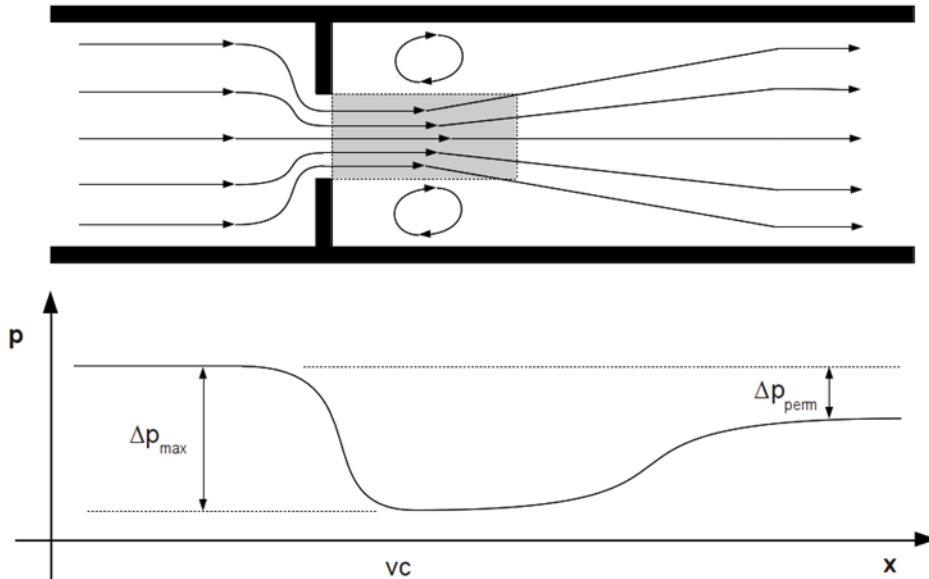


Figure 2. 16 Sketch of streamlines and pressure profile for flow through a circular orifice in a pipe. (Adapted from van der Zande et al., 1999).

The drop breakup experiments through this type of geometry started with Percy and Sleicher (1983). They have experimentally determined the maximum stable diameter d_m of a diluted Oil/Water mixture in flow through an orifice. They showed that the droplet diameter is correlated with the maximum pressure drop through the restriction, Δp_{max} , supposing that the deformation of the drop is related to the acceleration of fluid at the entrance of the orifice. They then defined the stress responsible for the deformation of a drop of diameter d as:

$$\tau = \frac{\Delta p_{max} d}{D_0} \quad (2.28)$$

These authors lead to an expression of the form:

$$d_m = k^* \sqrt{\frac{D_0 \sigma}{\Delta p_{max}}} \quad (2.29)$$

Where k^* is a constant. Percy and Sleicher have tested different experimental conditions (different orifice to tube diameter ratios, velocities and

Reynolds numbers) always in turbulent flow, and determined a value of 3.1 for constant k^* .

Then, van der Zande and van der Broek (1998) tested the correlation given by Equation 2.29 for another range of experimental conditions, finding a value of 5.4 for constant k^* . They also found that k^* decreases when the root term of Equation 2.29 increases. In posterior investigations, van der Zande et al. (1999) concluded that the breakup mechanism described by Percy and Sleicher was not the dominant mechanism (acceleration at the entrance of the restriction). Consequently, Equation 2.29 could not be used for the prediction of the maximum stable drop diameter, to the extent that k^* must be adjusted according to the operating conditions. In the same study, van der Zande et al. showed that drop breakup in a restriction is caused by the turbulent velocity fluctuations in the high velocity zone downstream of the restriction, and that the maximum stable drop diameter was (aside from the fluid properties) a function of the average energy dissipation rate per unit mass $\bar{\epsilon}$, given by Equation 2.27.

Later, Galinat et al. (2005) carried out an experimental analysis of drop breakup in turbulent pipe flow downstream of a restriction using a high-speed trajectography technique. They first performed a global analysis of the fragmentation process for a dilute dispersion, observing that the mean drop diameter downstream of the restriction linearly increases as a function of the inverse of the square root of the pressure drop, results that are in agreement with the previous experiences of Percy and Sleicher. In addition, experiments based on the observation of single drop breakup downstream of the orifice have allowed the identification of different breakup mechanisms, and the determination of statistical quantities such as the breakup probability, the mean number of fragments and the daughter drop distribution.

An experimental study coupled to a theoretical analysis of the breakup process in diluted medium downstream of an orifice (Tjaberinga, Boon and Chesters, 1993), shows that the diameter of the drops upstream of the orifice has little effect on the average droplet size produced in passing through the restriction. The numerical prediction of the droplet diameter downstream of the orifice is achieved by coupling a model of viscous rupture (critical capillary number) and a model of inertial rupture (critical Weber number in turbulent flow) to a CFD code (Turbulence modeled by a standard $k - \epsilon$ model). Nevertheless, constants must be

adjusted and the proposed models must be adapted to achieve a good agreement between simulations and experiments. However, this study was a promising first test modeling of the effect of a restriction on a diluted population of drops in turbulent flow.

Galinat et al. (2007) reported experimental and numerical results of the breakup probability of a drop travelling through inhomogeneous turbulent flow generated in a pipe downstream of a restriction, where various Reynolds numbers, damping coefficients and drop volume fractions were tested. The model coupled the Rayleigh–Lamb theory of drop oscillations with the Kolmogorov–Hinze theory of turbulent breakup. The interface deformation was modelled by a linear oscillator forced by the Lagrangian turbulent Weber number measured in the experiments. The rupture conditions appeared when the instantaneous Weber number exceeded a critical value or the predicted deformation exceeded a given threshold. Their simulations (assuming a critical deformation) predicted well the main features observed in the experiments and the linear oscillator was able to describe the main feature of the dynamics of the drop deformation in inhomogeneous turbulence. In addition, the model was used to compute the breakup probability in concentrated dispersed two-phase flows when the oscillation frequency and the damping rate were provided.

Recently, Maniero et al. (2012) numerically modeled the drop breakup at the same turbulent conditions as described by Galinat et al. (2007) by coupling Direct Numerical Simulation (DNS) of the continuous phase, Lagrangian droplet tracking, a dynamic model of drop deformation and a breakup criterion based on a maximal deformation. The dynamical model is adapted from the Kolmogorov – Hinze theory of turbulent breakup to the Rayleigh – Lamb theory of drop oscillations. Compared to PIV measurements, DNS results have demonstrated to provide a reliable prediction of the turbulent flow field and its statistics at the drop size scale; also, experimental breakup locations have been correctly predicted by adjusting only the critical deformation for breakage.